CrossMark

Layer-by-layer assembled graphene-coated mesoporous SnO$_2$ spheres as anodes for advanced Li-ion batteries

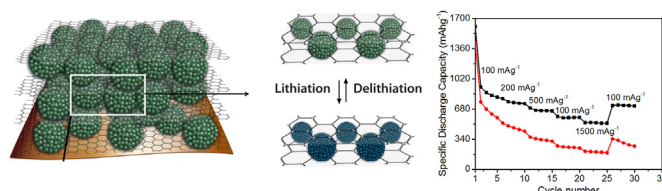Muhammad Shahid [a], Nulati Yesibolati [a], M.C. Reuter [b], F.M. Ross [b], H.N. Alshareef [a],*

[a] Materials Science and Engineering, King Abdullah University of Science and Technology (KAUST), Thuwal 23955-6900, Saudi Arabia
[b] IBM T.J. Watson Research Center, 1101 Kitchawan Road, Yorktown Heights, NY 10598, USA

HIGHLIGHTS

- Synthesis of LBL assembly of graphene/carbon-coated mesoporous SnO$_2$ spheres.
- Binder and additives free electrodes as anode materials for lithium ion batteries.
- The LBL assembled electrodes possess high reversible Li storage capacity.
- LBL assembled electrodes show excellent rate capability at high specific current.

GRAPHICAL ABSTRACT

ARTICLE INFO

ABSTRACT

We report layer-by-layer (LBL) assembly of graphene/carbon-coated mesoporous SnO$_2$ spheres (Gr/C-SnO$_2$ spheres), without binder and conducting additives, as anode materials with excellent Li-ion insertion–extraction properties. Our results indicate that these novel LBL assembled electrodes have high reversible Li storage capacity, improved cycling, and especially good rate performance, even at high specific currents. The superior electrochemical performance offered by these LBL assembled Gr/C-SnO$_2$ spheres is attributed to the enhanced electronic conductivity and effective diffusion of Li ions in the interconnected network of nanoparticles forming the mesoporous SnO$_2$ spheres.

© 2014 Elsevier B.V. All rights reserved.

1. Introduction

Lithium-ion batteries (LIBs) are considered excellent energy storage devices due to their high energy density, cycling stability and rate capability, with many potential applications such as portable electronic devices, hybrid electric vehicles, tablet PCs and notebooks [1–4]. In this respect various materials have been investigated as anode materials for lithium ion batteries [5–7]. Among these, tin

oxide (SnO$_2$) is considered as one of the most attractive Li$^+$ insertion anode materials to replace graphite in next generation Li-ion batteries due to its high theoretical capacity (782 mAh g^{-1}) and low discharge potential [8–10]. However, it is well known that the huge volumetric expansion/shrinkage due to the alloying/dealloying reactions of SnO$_2$ with lithium causes severe mechanical disintegration (such as cracking and pulverization), breakdown of the electrical conduction pathways in the electrodes, and even the loss of physical and electronic integrities of the active material which consequently degrades device performance [11–13]. In order to solve these major technical challenges, we have employed a double protection approach. We have developed a multi-component

---

* Corresponding author. Tel.: +966 (0) 12 808 4477.
E-mail address: husam.alshareef@kaust.edu.sa (H.N. Alshareef).

material that includes multiple layers of mesoporous SnO$_2$ spheres, each coated with a thin carbon layer, and that are sandwiched between layers of graphene. The material is fabricated using a simple and scalable hierarchical bottom-up layer-by-layer (LBL) assembly approach, shown in Fig. 1. The graphene layers not only provide electronic conductivity and flexibility, but also can accommodate the mechanical stress induced by the substantial volume expansion and shrinkage of the high-capacity SnO$_2$ spheres [14–16]. The thin layer of carbon coating on each SnO$_2$ sphere provides additional stability and conducting paths during lithium insertion and extraction [17,18]. Furthermore, this design maximizes the utilization of the SnO$_2$ by structuring it in the form of mesoporous spheres that are composed of interconnected nanoparticles, thereby significantly increasing the surface area available for efficient reaction of lithium with the SnO$_2$ anode. An advantage of this design is that polymer binders and conductive additives which are commonly used for other electrode materials are not needed, improving the overall energy density of the batteries.

2. Experimental

2.1. Materials preparation

Tin(IV) chloride pentahydrate (98%), D-glucose (99.9%), graphite powder, sulfuric acid, hydrazine hydrate, ammonium hydroxide, and ethanol (90%) were all purchased from Sigma Aldrich and used as received. Carbon coated mesoporous SnO$_2$ spheres were synthesized in three steps. In the first step, SnO$_2$ nanoparticles was synthesized via a hydrothermal method [19]. In a typical reaction, 7 g of SnCl$_4$·5H$_2$O (0.5 M) was dissolved in 40 ml of distilled water (DI water) under vigorous stirring for 1 h. The solution was then sealed in a teflon lined autoclave and kept in a furnace at 180 °C for 2 h. The obtained nanoparticles, were filtered, washed and dried. In the second step, SnO$_2$ spheres were prepared. 0.2 g of as-prepared SnO$_2$ nanoparticles were dispersed in 40 ml DI water, followed by adding 1 g of D-glucose. Then the mixture was continuously stirred for 2 h and transferred to a teflon lined autoclave and kept in the furnace at 180 °C for 6 h. This was resulted in the formation of the carbon layer and SnO$_2$ spheres, which was composed of an

assembly of about 10 nm nanoparticles (Fig. S1). These spheres were washed with water and ethanol and dried in a vacuum oven overnight. In order to prepare well shaped and uniform sphere structure, different hydrothermal synthesis time were conducted. We observed that the growth of spheres started within the first 4 h and was completed in 6 h; moreover, if the reaction time was more than 6 h the mesoporous nature of the spheres diminishes and they were converted to agglomerated, non-porous spheres as shown in supporting information (Fig. S2). In the third step, to improve the crystallinity of the carbon layer, annealing was performed at 500 °C in N$_2$ atmosphere for 4 h, after which the black color powder was successfully achieved. The well-shaped sphere structure around 1 μm could be confirmed from SEM (Fig. 2a and b). The mesoporous sphere structure is further investigated through TEM images which is composed of an assembly of about 10 nm nanoparticles as shown in Fig. 2 d and e Graphene was produced by the reduction of graphite oxide, which was prepared by an original Hummers method (SI, Preparation of graphene).

2.2. Electrode preparation

The LBL assembly of graphene/C-coated mesoporous SnO$_2$ spheres (Gr/C-SnO$_2$) into electrodes was carried out using the vacuum filtration (VF) method on a porous alumina membrane filter (0.2 μm pore size and 25 mm diameter; Whatman). The C-coated mesoporous SnO$_2$ spheres and graphene were dispersed separately in DI water and ultrasonicated for 1 h, resulting in concentrations of both solutions of 0.25 mg mL^{-1} for electrode assembly. Each layer of the composite layered electrodes was formed by vacuum filtration of 1 mL solution of either graphene or C-coated mesoporous SnO$_2$ spheres. By this method, the number of layers and concentration of each layer could be optimized. First the graphene solution was filtered by passing through the porous alumina membrane pores, trapping the graphene on the membrane surface, forming a homogeneous layer. Next the C-coated SnO$_2$ mesoporous spheres solution was filtered placing the spheres on the graphene surface. We realized that more layers would pulled off the electrode from the porous alumina membrane template as shown in supporting information (Fig. S3). Hence, after filtration of
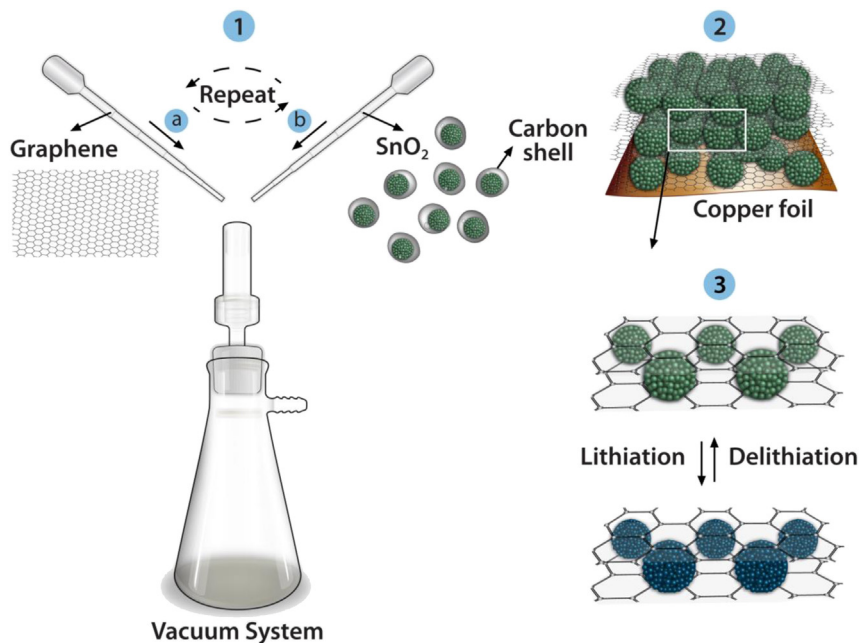

Fig. 1. Schematic view of the preparation of the assembled graphene/C-coated mesoporous SnO$_2$ spheres. Steps (1a) graphene and (1b) C-coated mesoporous SnO$_2$ spheres; Step (2) represents the LBL assembly on Cu foil. Step (3) represents lithiation and delithiation in the LBL assembly.
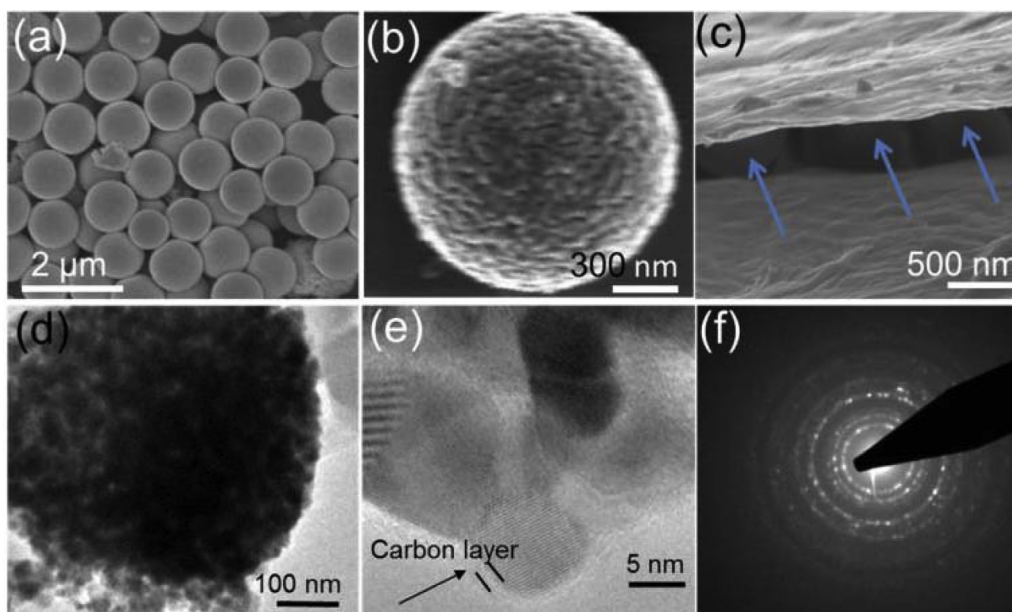
Fig. 2. (a) and (b) FE-SEM images of C-coated mesoporous SnO_2 spheres. (c) High resolution cross section SEM image showing spheres sandwiched between the graphene layers. (d) TEM image of spheres. (e) HRTEM image of a single nanocrystal. (f) SAED pattern of an individual carbon coated SnO_2 sphere.

9 layers (5 layers graphene, and 4 layers of C-coated mesoporous SnO_2 spheres), the prepared film was placed directly into a bath of 3 M NaOH solution. Finally, the porous alumina membrane was dissolved, and the thin Gr/C-SnO_2 sphere film was floated on the surface of the NaOH solution. The film was then transferred to a water bath. This step was repeated several times to remove NaOH traces. Finally, a piece of copper foil was immersed in the water bath allowing the film to transfer to the Cu foil. The as-formed electrodes were kept overnight at 80 °C in a vacuum oven for solvent evaporation. Fig. S4 shows the overall process involved in transferring the LBL assembled Gr/C-SnO_2 sphere electrode to the Cu foil. The LBL assembly of graphene SnO_2 nanoparticles electrode (Gr/SnO_2 NP) was also prepared via same procedures to compare the electrochemical performance with that of Gr/C-SnO_2 spheres electrodes. SnO_2 nanoparticles was previously synthesized (as described in the Experimental section).

2.3. Physical characterization

Structural analysis of the samples was performed with an X-ray diffraction system ((XRD, Bruker, D8 ADVANCE)) using Cu K$_\alpha$ radiation with a wavelength of 1.5418 Å Field emission scanning electron microscopy (FE-SEM, Nova Nano) and transmission electron microscopy (300 KV TEM, FEI-CM30) were used to investigate the morphology of the C-coated mesoporous SnO_2 spheres and electrodes. Surface area and pore size distribution measurement (ASAP 2420, surface area and pore size analyzer, Micromeritics) was carried out by nitrogen adsorption and desorption. Raman spectroscopic measurements were carried out using a LabRam Aramis Raman spectrometer with a He–Ne laser having an excitation wavelength of 633 nm. Thermogravimetric analysis (TGA) was performed using a TG 209 F1 Iris system at a heating rate of 5 °C min^{-1} in flowing air.

2.4. Electrochemical characterization

The electrochemical measurements were performed using coin cells (CR2032, MTI) in the voltage range of 0.005–3.00 V, with Li metal as the counter and reference electrode. The electrolyte was a mixture of lithium salt and organic solvents. The LiPF$_6$ was

dissolved in ethylene carbonate (EC)/diethylene carbonate (DEC) (1:1, by weight) to obtain the electrolytic solution of 1 M LiPF$_6$ about 0.2 mL of electrolyte was used in each experiment. The coin cells were assembled in an argon-filled glove box (MBRAUN) with oxygen and moisture less than 0.1 ppm. Charge/discharge tests were performed at various specific currents using a Bio-logic VMP3 EC-Lab system. Electrochemical impedance spectroscopy (EIS) was performed by applying a sine wave with an amplitude of 5.0 mV over the frequency range of 1000 kHz–0.01 Hz at open circuit voltage (OCV states) before electrochemical cycle.

3. Results and discussion

Fig. 2a–c shows the surface morphologies of the spheres and the LBL assembly of the Gr/C-SnO_2 spheres electrode, investigated by FE-SEM. The FE-SEM images show that as-prepared carbon coated mesoporous structures are spherical in shape with an average diameter of 1 μm. The cross-sectional FE-SEM images of these Gr/C-SnO_2 spheres in Fig. 2c show that the spheres are uniformly sandwiched between the graphene sheets (marked by the arrows in the high resolution SEM image in Fig. 2c). Fig. S5 shows a top view of the LBL electrode, where the spheres are visible (marked by red circles) under the graphene layer. The uniformity and thickness of the carbon layer on the spheres was studied by high resolution TEM analysis. Fig. 2d and e shows that the as-prepared spheres composed of an assembly of nanoparticles have mesoporous structure. Fig. 2e shows an HRTEM image of SnO_2 nanocrystals, which confirmed the uniform carbon layer coated on the surface of nanoparticles. The thickness of the carbon layer is about 2 nm. Fig. 2f shows a SAED pattern which confirms the polycrystalline nature of the spheres.

Fig. 3a shows XRD patterns of SnO_2 nanoparticles, C-coated SnO_2 spheres after calcination at 500 °C, and the LBL film of Gr/C-SnO_2 spheres. All diffraction peaks are indexed as rutile SnO_2 (JCPDS card no. 41-1445) without any traces of other crystalline phases or byproducts. In order to confirm the coating of carbon over the SnO_2 spheres, we have done Raman analysis. The broadness of D and G band indicative of carbon coating which is amorphous nature. As it is amorphous, we could not find any diffraction signal while doing XRD. Raman spectra of the LBL assembly of Gr/C-
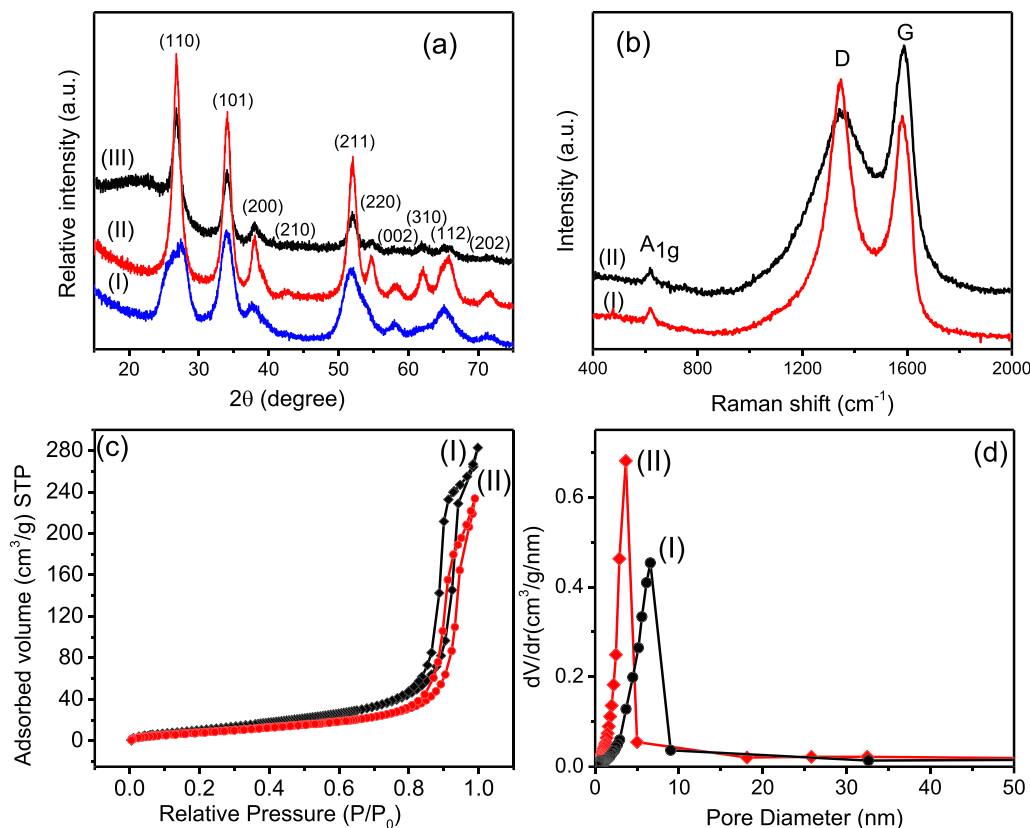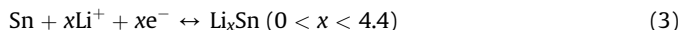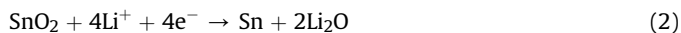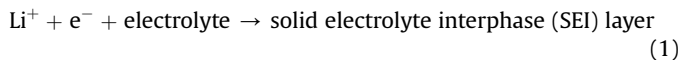
Fig. 3. (a) XRD patterns of the (I) as-prepared SnO_2 nanoparticles (II) C-coated mesoporous SnO_2 spheres after annealing at 500 °C for 4 h and (III) LBL assembly of Gr/C-SnO_2 spheres. (b) Raman spectra of (I) LBL assembly of Gr/C-SnO_2 spheres and (II) C-coated mesoporous SnO_2 spheres after annealing at 500 °C for 4 h. (c) Nitrogen adsorption–desorption isotherms curves for mesoporous SnO_2 before annealing (I) and carbon coated SnO_2 spheres (II) after annealing at the 500 °C for 4 h. (d) The pore size distributions for mesoporous SnO_2 before annealing (I) and carbon coated SnO_2 spheres after annealing (II).

SnO_2 spheres (red curve (in the web version), (I)) and carbon coated SnO_2 spheres (black curve, (II)) are shown in Fig. 3e. It can be seen that both materials show the D and G bands at around 1347 and 1587 cm^{-1} respectively. It is known that D band is related to graphene disordered structures and G band related to the graphene crystalline structure [20–22]. The peak found at 620 cm^{-1} in the Raman spectrum of the C-coated SnO_2 spheres and LBL assembly of Gr/C-SnO_2 spheres can be assigned to the A_{1g} active modes of crystalline SnO_2 [23].

The porous structure of the as prepared SnO_2 and carbon coated SnO_2 spheres after annealing at 500 °C, was investigated employing N_2 adsorption–desorption isotherms (shown in Fig. 3c). The plot corresponds to the type-IV isotherms hysteresis loops, which indicates the mesoporous nature of the samples. The surface area of mesoporous SnO_2 spheres, black curve, (I) exhibited 73.53 m^2 g^{-1} while the red curve (II) after annealing shows a surface area of 56.88 m^2 g^{-1}. According to the BET results, as prepared spheres have a slightly large pore diameter as compared to the annealed SnO_2 spheres (Fig. 3e), which may be due to the fact that carbon layer on SnO_2 surface leading to the shrinkage of pores upon calcination. Thermogravimetric analysis (TGA) was performed to quantitatively determine the amount of carbon present in the final products and the results are shown in supporting information (Fig. S6). It can be seen that weight loss takes place in the temperature between 300 and 900 °C implying that the anode material is composed of 45% carbon.

To evaluate the potential of the LBL assembly of Gr/C-SnO_2 spheres in Li ion batteries, we investigated their electrochemical response with respect to Li insertion–extraction. Furthermore, we compared the performance of LBL assembly of Gr/C-SnO_2 spheres

to the LBL assembly of graphene/SnO_2 nanoparticles (Gr/SnO_2 NP). Fig. 4a and b shows the first three cyclic voltammogram (CV) curves of LBL assembled Gr/C-SnO_2 NP and LBL Gr/C-SnO_2 sphere electrode respectively. The CV was conducted at a scan rate of 0.2 mV s^{-1} from 3 to 0.005 V. As can be seen from Fig. 4a and b, the profiles of these curves are in good agreement with the electrochemical behavior of SnO_2-based anodes as reported in literature [24,25].

$$Li^+ + e^- + \text{electrolyte} \rightarrow \text{solid electrolyte interphase (SEI) layer} \tag{1}$$

$$SnO_2 + 4Li^+ + 4e^- \rightarrow Sn + 2Li_2O \tag{2}$$

$$Sn + xLi^+ + xe^- \leftrightarrow Li_xSn \ (0 < x < 4.4) \tag{3}$$

In the first cycle, Fig. 4a, LBL Gr/SnO_2 NP electrode displays a strong reduction peak at approximately 0.85 V, which is assigned to the reduction of SnO_2 to Sn and the formation of solid electrolyte interphase (SEI) layers [26,27] as described in Eqs. (1) and (2). The SEI formation (Reaction (1)) is considered as a main irreversible process, which results in the large capacity loss during the initial cycle. Another broaden peak at 0.1 V can be represented to the formation of Li_xSn alloys [28]. In the oxidation curves, the peak at 0.55 V can be attributed to the dealloying of Li from the Li–Sn alloy formed in the reductive sweep. This alloying/dealloying Li-storage described by Eq. (3) is considered to be highly reversible and dominantly contributes to the reversible lithium storage capacity. The relatively weak peak at about 1.2 V can be ascribed to the partial reversible of the second reaction [29] shown in Eq. (2). Several weak peaks
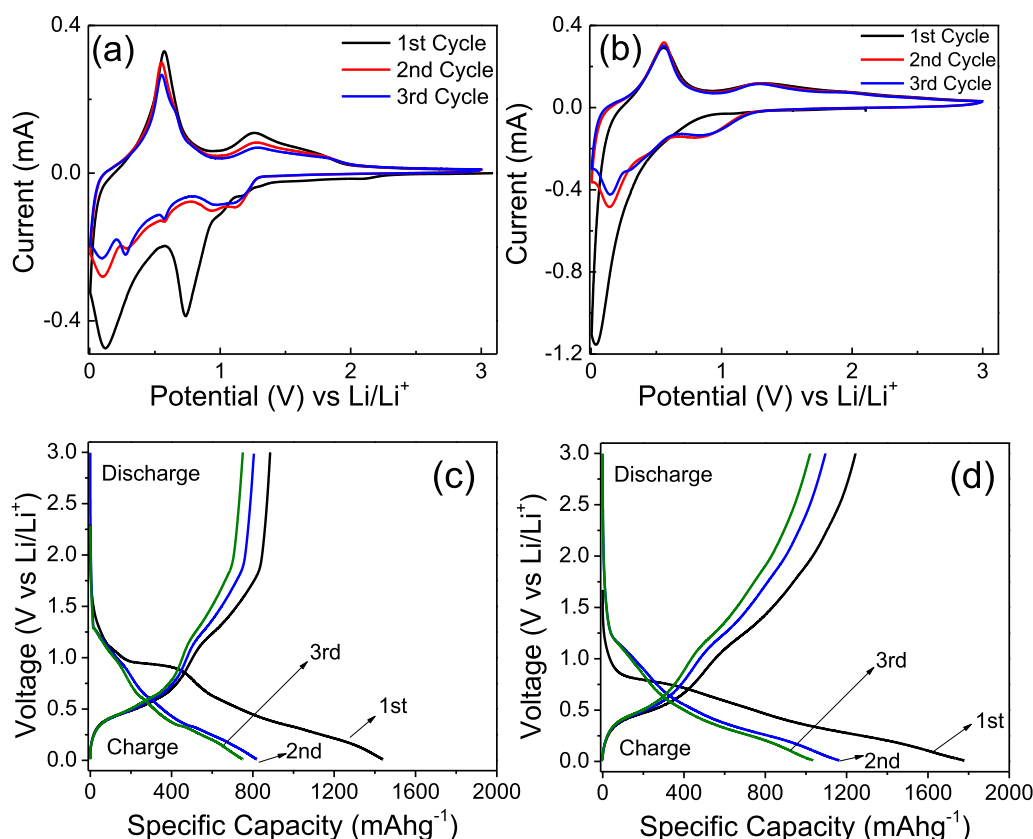
Fig. 4. (a) The first three CV curves for the Gr/SnO$_2$ NP and (b) Gr/C-SnO$_2$ spheres at a scan rate of 0.2 mV s^{-1} in the voltage range of 3–0.005 V. (c) Galvanostatic discharge–charge profiles for LBL electrode of Gr/SnO$_2$ NP and (d) Gr/C-SnO$_2$ spheres at a specific current of 100 mA g^{-1} in the voltage range of 3–0.005 V.

between 0.05 and 0.55 V have been detected during the third reduction cycle, which could be assigned to the different level of alloying [30,31]. The intensity of the anodic peaks in Fig. 4a decreases drastically in the initial three cycles, indicating poor cycling stability of the LBL Gr/SnO$_2$ NP electrode. In contrast, the CV profile of the LBL Gr/C-SnO$_2$ spheres electrode shows the suppression of SEI formation. This indicates some hindrance of the electrolyte decomposition reaction during SEI formation at the equilibrium-potential range, which could improve the initial coulombic efficiency. Moreover, it is worth mentioning that the anodic peaks at 0.55 V almost overlap from the first to third cycles without negligible change, suggesting that the LBL Gr/C-SnO$_2$ sphere electrode has good electrochemical performance as compared to the G/SnO$_2$ NP electrode. In contrast with these CV results, correlative plateau regions and higher capacity can be observed in the charge–discharge voltage profiles of the LBL assembled Gr/C-SnO$_2$ spheres and the Gr/SnO$_2$ NP electrodes. Fig. 4c and d shows the discharge–charge profiles for the first three cycles at a specific current 100 mA g^{-1} between 0.005 V and 3 V for the LBL Gr/SnO$_2$ NP electrode and LBL Gr/C-SnO$_2$ spheres respectively. The LBL assembled Gr/C-SnO$_2$ sphere electrode shows large initial discharge and charge capacities of about 1783 and 1247 mAh g^{-1} (Fig. 4d) as compared to the LBL Gr/SnO$_2$ NP electrode shown in Fig. 4c, which was shown initial discharge capacity of 1437 mAh g^{-1} and charge capacity of 884 mAh g^{-1}. It is generally known that SnO$_2$ anodes show a dramatic loss in their initial charge capacity. This loss of the irreversible capacity is mainly due to the irreversible reduction of the formation of the SEI [32,33]. Fig. 5a shows the cycling performances of Gr/C-SnO$_2$ spheres and Gr/SnO$_2$ NP (specific capacity mAh g^{-1} vs cycle number) along with their coulombic efficiency. The first cycle coulombic efficiency Gr/C-SnO$_2$ spheres electrode is 69.9% which is

higher than most literature reports, which typically show an initial coulombic efficiency of SnO$_2$ lower than 60% [34]. The low coulombic efficiency of Gr/SnO$_2$ NP electrode for the first cycle is due to the formation of SEI and the continuous consumption of lithium, as there is no protecting layer on the surface of SnO$_2$ nanoparticles, thus more electrolyte can react with the bare SnO$_2$ nanoparticles surface and result in a low coulombic efficiency. The columbic efficiency reaches 99.9% after a few cycles, indicating highly reversible charge–discharge behavior. The LBL assembled Gr/C–SnO$_2$ electrode demonstrates excellent cycling performance compared to the Gr/SnO$_2$ NP electrode. Typically for anodes composed of SnO$_2$ NPs, the specific capacity fades rapidly [35–37]. This suggests that stress created during Li insertion–extraction in SnO$_2$ could result in cracking as well as loss of electronic connectivity between particles leading to poor cycling performance. The discharge capacity of Gr/C-SnO$_2$ sphere can be compared with capacities of graphene/SnO$_2$-based anodes reported in the literature previously, and the relevant data are presented in supporting information Table S1. All capacities are taken from the 50th cycle in the corresponding experiments. In order to compare the performance of the reported literature with our materials correctly, we take into account that all the electrodes are binder and conductive additives free as shown in Table S1. We have obtained a capacity of 502 mAh g^{-1} at a specific current of 100 mA g^{-1} for the Gr/C-SnO$_2$ spheres, which is almost 150% higher than the Gr/SnO$_2$ NP electrode at the same specific current. Fig. 5b shows the rate capability of the LBL assembled Gr/C-SnO$_2$ sphere and Gr/SnO$_2$ NP electrodes (Fig. S7, Supporting information is the plot of variation of the specific discharge capacity with specific current). It can be observed from Fig. 5b that the difference between the specific capacities of the LBL assembled Gr/C-SnO$_2$ spheres and Gr/SnO$_2$ NP increases significantly by increasing scan rate. A reversible capacity
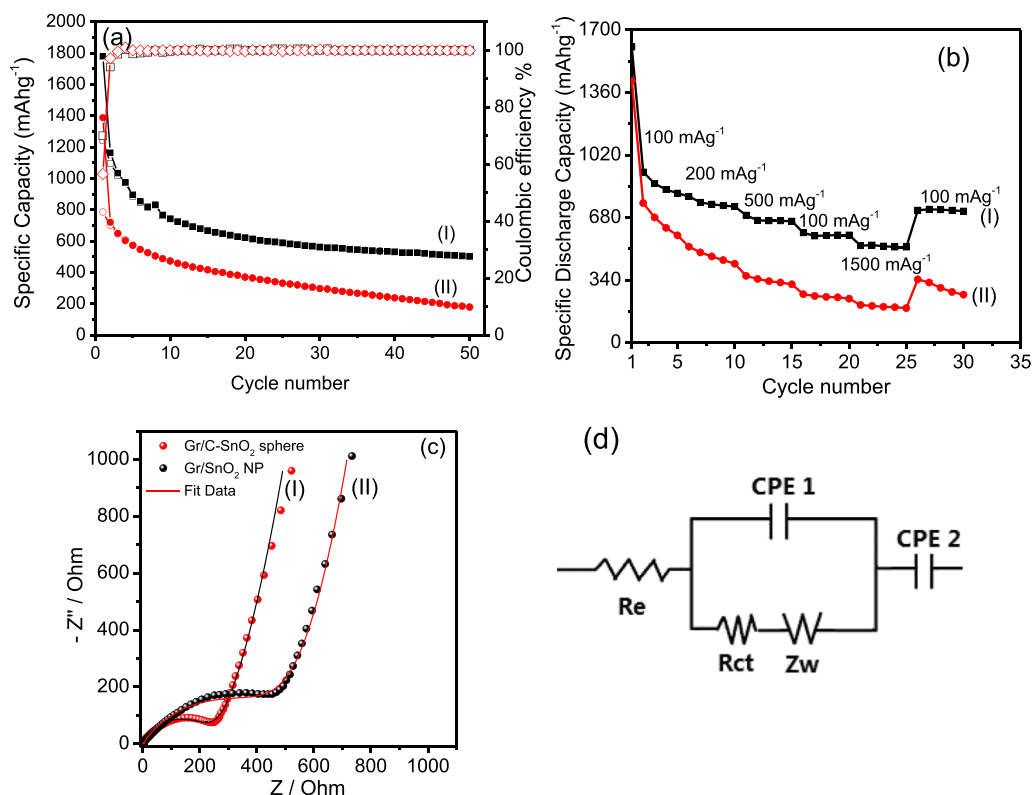
Fig. 5. (a) Cycling performance and coulombic efficiency of (I) Gr/C-SnO$_2$ spheres and (II) Gr/SnO$_2$ NP up to 50 cycles at 100 mA g^{-1} specific currents. (b) Discharge capacity of the LBL assembly of (I) Gr/C-SnO$_2$ spheres and (II) Gr/SnO$_2$ NP electrode at different specific currents. (c) Nyquist plots for Gr/C-SnO$_2$ spheres (I) and Gr/SnO$_2$ NP (II) electrodes. (d) The Randles equivalent circuit for Gr/C-SnO$_2$ spheres and Gr/SnO$_2$ NP electrode.

of 520 mAh g^{-1} was observed at a high current rate of 1500 mA g^{-1}, demonstrating an outstanding high-rate performance. When the cycling current rate was again reduced back to 100 mA g^{-1}, the electrode can still provide a high reversible capacity of 720 mAh g^{-1}, indicating that the structure of the electrode remains stable even under the high rate cycling. We believe that the improved capacity retention in our LBL assembled Gr/C-SnO$_2$ spheres could be due to several factors. Firstly, the carbon layer on the mesoporous SnO$_2$ spheres after carbonization becomes highly electronically conductive, which helps to increase the reversibility of lithium ion insertion. Secondly, the thin covering of graphene sheets on the carbon-coated SnO$_2$ spheres and on the NPs should improve their electronic conductivity. Thirdly, the graphene itself could store the Li ions and the LBL assembly can prevent the aggregation and cracking of the spheres upon lithiation. Finally, the mesoporous nature of the C-coated SnO$_2$ spheres make it possible for the electrolyte to diffuse into the spheres to access all the SnO$_2$ while sustaining their structure. This is mainly due to the porosity between the particles that make up the SnO$_2$ spheres, which buffers the large volume change during lithium ion insertion and extraction.

In order to elucidate the effect of the carbon layer on the electrochemical performance of Gr/C-SnO$_2$ spheres, we have calculated theoretically the capacity of the Gr/C-SnO$_2$ sphere electrode from the theoretical capacities of the fully lithiated composition, Li$_{4.4}$Sn (994 mAh g^{-1}) and the graphite (372 mAh g^{-1}) [38,39] for comparison. However, we have calculated the capacity based on the composite weight i.e., SnO$_2$, carbon and graphene which is 714 mAh g^{-1}. The composition of the SnO$_2$ and carbon is about 55% and 45%, respectively based on TGA experiment. We have used the following formula [40] to calculate the theoretical capacity: $C_{\text{theoretical}} = C_{\text{SnO}_2} \times$ % mass of SnO$_2$ + $C_{\text{graphite}} \times$ % mass of graphite

$994 \times 0.55 + 372 \times 0.45 = 714$ mAh g^{-1}. We have obtained stable capacity of 502 mAh g^{-1} which is below the theoretical capacity of 714 mAh g^{-1} considering both SnO$_2$ and carbon material weight together. The initial discharge capacity of our Gr/C-SnO$_2$ spheres and Gr/SnO$_2$ NP electrode was 1783 and 1437 mAh g^{-1} respectively were obtained in the first cycle. The high discharge capacity in the initial cycles could be due to the irreversible reduction of SnO$_2$ to Sn and the formation of the SEI. The EIS studies of the Gr/C-SnO$_2$ spheres (I) and Gr/SnO$_2$ NP (II) are presented as Nyquist plots (Z′ vs. −Z″), where Z′ and Z″ refer to the real and imaginary parts of cell impedance, respectively (Fig. 5c). The typical characteristics of the two Nyquist plots are one semicircle in the medium frequency range and a straight line in the low frequency range. No semicircles were detected in the high frequency range in both electrodes. The semicircles in high frequencies usually could be attributed to the grain, grain boundary and SEI resistance [41,42]. The absence of a semicircle at high frequencies in the plots (Fig. 5c) suggests that no interface exist on the surface of electrodes as impedance experiments were conducted before electrochemical cycle. The equivalent circuit model of the studied system is shown in Fig. 5d to represent the internal resistance of the test battery, according to the literature [43–45]. R_e is the electrolyte resistance; R_{ct} is charge-transfer resistance. Z_w is the warburg impedance related to the lithium ions diffusion into the bulk electrodes and CPE represents the constant phase element. It can be seen, after coating carbon the Gr/C-SnO$_2$ spheres electrodes (I) possess significantly lower charge-transfer resistance than Gr/SnO$_2$ NP (II) see Table S2. This result also validates that the introduction of carbon layers can improve the electrical conductivity [46,47] of the overall electrode, thus greatly enhance rapid electron transport and its porous structure could allow fast lithium insertion/

extraction, resulting in significant improvement in the electrochemical performances.

4. Conclusions

A unique graphene/SnO_2 Li-ion battery anode has been designed and tested, which is composed of C-coated mesoporous SnO_2 spheres synthesized by a hydrothermal method. The C-coated mesoporous SnO_2 spheres were assembled between graphene nanosheets by vacuum filtration. The experimental results show that LBL assembled Gr/C-SnO_2 spheres exhibited better electrochemical performance compared to LBL assembled Gr/SnO_2 nanoparticles due to their lower contact and charge-transfer resistance. We conclude that LBL assembled Gr/C-SnO_2 spheres show great promise as anode materials for the next-generation lithium-ion batteries.

Acknowledgments

Appendix A. Supplementary data

Supplementary data related to this article can be found at http://dx.doi.org/10.1016/j.jpowsour.2014.03.146.

References

[1] H. Wu, Y. Cui, Nano Today 7 (2012) 414–429.
[2] G. Zhou, D.-W. Wang, F. Li, L. Zhang, N. Li, Z.-S. Wu, L. Wen, G.Q. Lu, H.-M. Cheng, Chem. Mater. 22 (2010) 5306–5313.
[3] Y. Li, B. Tan, Y. Wu, Nano Lett. 8 (2008) 265–270.
[4] C.-H. Lai, K.-W. Huang, J.-H. Cheng, C.-Y. Lee, B.-J. Hwang, L.-J. Chen, J. Mater. Chem. 20 (2010) 6638–6645.
[5] K.T. Nam, D.-W. Kim, P.J. Yoo, C.-Y. Chiang, N. Meethong, P.T. Hammond, Y.-M. Chiang, A.M. Belcher, Science 312 (2006) 885–888.
[6] J.-H. Cho, S.T. Picraux, Nano Lett. 13 (2013) 5740–5747.
[7] Y. Sun, J. Wang, B. Zhao, R. Cai, R. Ran, Z. Shao, J. Mater. Chem. A 1 (2013) 4736–4746.
[8] J. Liang, Z. Cai, Y. Tian, L. Li, J. Geng, L. Guo, ACS Appl. Mater. Interfaces 5 (2013) 12148–12155.
[9] X. Wang, X. Cao, L. Bourgeois, H. Guan, S. Chen, Y. Zhong, D.-M. Tang, H. Li, T. Zhai, L. Li, Y. Bando, D. Golberg, Adv. Funct. Mater. 22 (2012) 2682–2690.
[10] J. Xie, S.-Y. Liu, X.-F. Chen, Y.-X. Zheng, W.-T. Song, G.-S. Cao, T.-J. Zhu, X.-B. Zhao, Int. J. Electrochem. Sci. 6 (2011) 5539–5549.
[11] J.Y. Huang, L. Zhong, C.M. Wang, J.P. Sullivan, W. Xu, L.Q. Zhang, S.X. Mao, N.S. Hudak, X.H. Liu, A. Subramanian, H. Fan, L. Qi, A. Kushima, J. Li, Science 330 (2010) 1515–1520.
[12] T. Moon, C. Kim, S.-T. Hwang, B. Park, Electrochem. Solid-State Lett 9 (2006) A408–A411.
[13] T. Brousse, R. Retoux, U. Herterich, D.M. Schleich, J. Electrochem. Soc. 145 (1998) 1–4.
[14] X. Zhou, Y.-X. Yin, L.-J. Wan, Y.-G. Guo, J. Mater. Chem. 22 (2012) 17456–17459.
[15] S.-K. Park, S.-H. Yu, N. Pinna, S. Woo, B. Jang, Y.-H. Chung, Y.-H. Cho, Y.-E. Sung, Y. Piao, J. Mater. Chem. 22 (2012) 2520–2525.
[16] Y. Sun, Q. Wu, G. Shi, Energy Environ. Sci. 4 (2011) 1113–1132.
[17] J. Liu, W. Li, A. Manthiram, Chem. Commun. 46 (2010) 1437–1439.
[18] X. Ji, X. Huang, J. Liu, J. Jiang, X. Li, R. Ding, Y. Hu, F. Wu, Q. Li, Nanoscale Res. Lett. 5 (2010) 649–653.
[19] J.S. Chen, Y.L. Cheah, Y.T. Chen, N. Jayaprakash, S. Madhavi, Y.H. Yang, X.W. Lou, J. Phys. Chem. C 113 (2009) 20504–20508.
[20] F. Li, J. Song, H. Yang, S. Gan, Q. Zhang, D. Han, A. Ivaska, L. Niu, Nanotechnology 20 (2009) 455602–455608.
[21] Y. Li, X. Lv, J. Lu, J. Li, J. Phys. Chem. C 114 (2010) 21770–21774.
[22] Y. Li, S. Zhu, Q. Liu, J. Gu, Z. Guo, Z. Chen, C. Feng, D. Zhang, W.-J. Moon, J. Mater. Chem. 22 (2012) 2766–2773.
[23] S.H. Sun, G.W. Meng, G.X. Zhang, T. Gao, B.Y. Geng, L.D. Zhang, J. Zuo, Chem. Phys. Lett. 376 (2003) 103–107.
[24] L. Zhang, H.B. Wu, B. Liu, X.W. Lou, Energy Environ. Sci. 7 (2014) 1013–1017.
[25] F. Han, W.-C. Li, M.-R. Li, A.-H. Lu, J. Mater. Chem. 22 (2012) 9645–9651.
[26] X. Yin, L. Chen, C. Li, Q. Hao, S. Liu, Q. Li, E. Zhang, T. Wang, Electrochim. Acta 56 (2011) 2358–2363.
[27] X. Wang, Z. Li, Q. Li, C. Wang, A. Chen, Z. Zhang, R. Fan, L. Yin, CrystEngComm 15 (2013) 3696–3704.
[28] D.M. Bailey, W.H. Skelton, J.F. Smith, J. Less-Common Met. 64 (1979) 233–239.
[29] D. Wang, J. Yang, X. Li, D. Geng, R. Li, M. Cai, T.-K. Sham, X. Sun, Energy Environ. Sci. 6 (2013) 2900–2906.
[30] F.D. Lupo, C. Gerbaldi, G. Meligrana, S. Bodoardo, N. Penazzi, Int. J. Electrochem. Sci. 6 (2011) 3580–3593.
[31] I.A. Courtney, J.R. Dahn, J. Electrochem. Soc. 144 (1997) 2045–2052.
[32] W.-M. Zhang, J.-S. Hu, Y.-G. Guo, S.-F. Zheng, L.-S. Zhong, W.-G. Song, L.-J. Wan, Adv. Mater. 20 (2008) 1160–1165.
[33] X.W. Lou, J.S. Chen, P. Chen, L.A. Archer, Chem. Mater. 21 (2009) 2868–2874.
[34] R. Hu, W. Sun, H. Liu, M. Zeng, M. Zhu, Nanoscale 5 (2013) 11971–11979.
[35] P. Lian, X. Zhu, S. Liang, Z. Li, W. Yang, H. Wang, Electrochim. Acta 56 (2011) 4532–4539.
[36] J. Xie, J. Yang, X. Zhou, RSC Adv. 4 (2014) 572–577.
[37] L.-S. Zhang, L.-Y. Jiang, H.-J. Yan, W.D. Wang, W. Wang, W.-G. Song, Y.-G. Guo, L.-J. Wan, J. Mater. Chem. 20 (2010) 5462–5467.
[38] Y.-D. Ko, J.-G. Kang, J.-G. Park, S. Lee, D.-W. Kim, Nanotechnology 20 (2009) 455701–455707.
[39] Y.-G. Guo, J.-S. Hu, L.-J. Wan, Adv. Mater. 20 (2008) 2878–2887.
[40] S.-M. Paek, E. Yoo, I. Honma, Nano Lett. 9 (2009) 72–75.
[41] Y.-X. Wang, Y.-G. Lim, M.-S. Park, S.-L. Chou, J.H. Kim, H.-K. Liu, S.-X. Dou, Y.-J. Kim, J. Mater. Chem. A 2 (2014) 529–534.
[42] P. Singh, J.B. Goodenough, J. Am. Chem. Soc. 135 (2013) 10149–10154.
[43] D. Aurbach, M.D. Levi, E. Levi, H. Teller, B. Markovsky, G. Salitra, U. Heider, L. Heider, J. Electrochem. Soc. 145 (1998) 3024–3034.
[44] M.D. Levi, D. Aurbach, J. Phys. Chem. B 101 (1997) 4630–4640.
[45] M.D. Levi, K. Gamolsky, D. Aurbach, U. Heider, R. Oesten, Electrochim. Acta 45 (2000) 1781–1789.
[46] J.-J. Zhang, Z. Wei, T. Huang, Z.-L. Liu, A.-S. Yu, J. Mater. Chem. A 1 (2013) 7360–7369.
[47] G.-N. Zhu, C.-X. Wang, Y.-Y. Xia, J. Electrochem. Soc. 158 (2011) A102–A109.